Bull. Chem. Soc. Ethiop. **2019**, 33(1), 113-125.
DOI: https://dx.doi.org/10.4314/bcse.v33i1.11

ISSN 1011-3924
Printed in Ethiopia

EFFECT OF SYNTHESIZED TEMPERATURE ON THE ASSEMBLY AND PROPERTIES OF FOUR LANTHANIDE SUPRAMOLECULAR FRAMEWORKS

Yang Luo[1], Jie Wan[2], Yi-Feng Xiong[1], Lu Lu[1*], Guang-Li Wang[1], Xin-Yu Ling[1], Ya-Ting Hu[3], Qian-Yi Chen[3] and Ying Pan[3*]

[1]School of Chemistry and Environmental Engineering, Sichuan University of Science & Engineering, Zigong, China
[2]School of Basic Medicine, Guangdong Medical University, Dongguan, 523808, China
[3]Dongguan Key Laboratory of Drug Design and Formulation Technology, Key Laboratory of Research and Development of New Medical Materials of Guangdong Medical University, School of Pharmacy, Guangdong Medical University, Dongguan, 523808, China

(Received September 14, 2018; Revised January 17, 2019; Accepted January 24, 2019)

ABSTRACT. Four new lanthanide coordination polymers, $[H_3O][Ln_3(HPA)_{10}(H_2O)_3{\cdot}2H_2O]$ (Ln = Pr for **1**, Ln = Nd for **2**), $[Ln_2(HPA)_6(H_2O)_4{\cdot}2H_2O]$ (Ln = Sm for **3**, Ln = Tb for **4**) (HHPA =3-(4-hydroxyphenyl)propanoic acid), were successfully synthesized and characterized. **1** and **2** are isostructural and have 1D metal chain structure, while **3** and **4** show 0D network with binuclear subunits. The results indicated that the effect of reaction temperature can modulate the final structures. The HPA ligands adopt bidentate chelating and tridentate chelating bridging modes to coordinate with Ln(III) ions in **1**-**4**. It has been shown that **4** can act as a fluorescent sensor for highly sensitive detection of nitroaromatics and Fe^{3+}.

KEY WORDS: Sensor, Lanthanide, Structure, Temperature

INTRODUCTION

Coordination polymers (CPs) have attracted increasing interest because of their fascinating motifs and excellent applications in the fields of luminescence, catalysis, and drug delivery [1]. As we know, the construction of CPs is influenced by several factors, such as the central metal ions, organic carboxylate ligands, reaction temperature, and so on [2-3]. Any subtle change of one of the mentioned factors may lead to a drastic change in the dimensionality and properties [4]. Therefore, deliberate exploration of an assembling process with the fixed metal centers and organic linkers is crucial for gaining expected target product [5]. Temperature is still a challenge in determining the ultimate dimensionality of CPs among the concerned many factors.

Beyond that trivalent lanthanide ions are outstanding in fluorescence applications because of their high color purity due to the 4f-shell electronic transitions [8]. Benzoic acid and some of its derivatives are often used as catalyst precursor polymers in pharmaceutical industries, and important organic ligands to construct complexes with lanthanide metal ions [9]. Fortunately, through adjusting the reaction temperatures, we successfully prepared four Ln(II) CPs based on the 3-(4-hydroxyphenyl)propanoic acid ligands. **1** and **2** are isostructural and have 1D metal chain structure, while **3** and **4** show 0D network with binuclear subunits. Synthesis, structures, and luminescent sensing properties were investigated.

EXPERIMENTAL

All the other reagents used for the syntheses were commercially available and employed without further purification. Powder X-ray diffraction (PXRD) was collected on a Bruker D8 Advance X-ray diffractometer with Cu-Kα radiation (λ = 1.5418 Å) at 50 kV, 20 mA with a scanning rate

*Corresponding author. E-mail: lulusczg@126.com; ying-p@163.com

of 6°/min and a step size of 0.02°. Fourier transform infrared (FT-IR) spectra as KBr pellets were measured using a Nicolet Impact 750 FTIR in the range of 400-4000 cm^{-1}. Thermogravimetric analysis was performed under N_2 atmosphere from room temperature to 900 °C at a heating rate of 10 °C min^{-1}.

The photoluminescence sensing were performed as follows: the photoluminescence properties of **4** were investigated in water emulsions at room temperature using a RF-5301PC spectrofluorophotometer. The emulsions were prepared by adding 3 mg of **4** powder into 3.00 mL of water and then ultrasonic agitation the mixture for 30 min before testing.

X-Ray crystallography

Single crystal X-ray diffraction data collection were collected on a Bruker SMART APEX diffractometer that was equipped with graphite monochromated Mo-Kα radiation (λ = 0.71073 Å) by using an ω-scan technique at 100 K. The intensities were corrected for absorption effects by using SADABS. The structure was solved using SHELXL-97 [10]. All the hydrogen atoms were generated geometrically and refined isotropically using a riding model. All non-hydrogen atoms were refined with anisotropic displacement parameters. Crystallographic details and selected bond dimensions for **1-4** are listed in Tables 1-2, respectively. CCDC numbers: 1849840-1849843.

Syntheses

*$[H_3O][Pr_3(HPA)_{10}(H_2O)_3{\cdot}2H_2O]$ (**1**)*. 20 mL solution of HHPA (0.125 g, 0.75 mmol) in CH_3OH:H_2O (v/v = 1:1) was added to an aqueous solution of $Pr(NO_3)_3{\cdot}6H_2O$ (0.33 g, 0.75 mmol) and then the mixture was heated to 80 ºC for 30 min. The pH of the resulting solution was adjusted to 6 using triethylamine and kept at room temperature. Green block crystals of **1** were obtained in 62% yield based on Pr. Anal. calc. for $C_{90}H_{102}O_{36}Pr_3$ (%): C, 49.53; N, 0; H, 4.71. Found: C, 49.67; N, 0; H, 4.74.

Table 1. Crystal data and structure refinement information for **1-4**.

Compound	**1**	**2**	**3**	**4**
Empirical formula	$C_{90}H_{102}O_{36}Pr_3$	$C_{90}H_{102}Nd_3O_{36}$	$C_{54}H_{66}O_{24}Sm_2$	$C_{54}H_{66}O_{24}Tb_2$
Formula wt	2182.44	2192.44	1399.77	1416.91
Crystal system	Triclinic	Triclinic	Monoclinic	Monoclinic
space group	P-1	P-1	P21/c	P21/c
a (Å)	12.208(9)	12.207(3)	21.484(12)	21.42(3)
b (Å)	14.640(11)	14.696(4)	14.458(8)	14.394(18)
c (Å)	14.837(10)	14.858(4)	9.092(5)	9.030(11)
α [°]	92.738(14)	92.56	90.00	90.00
β [°]	104.232(13)	104.053(4)	95.376(12)	95.15(3)
γ [°]	97.363(15)	97.69	90.00	90.00
V ($Å^3$)	2541(3)	2554.2(12)	2812(3)	2772(6)
Z	1	1	2	2
ρ_{calc}[g·cm^{-3}]	1.426	1.425	1.653	1.698
μ (mm^{-1})	1.494	1.580	2.151	2.615
F(000)	1107	1110	1412	1424
θ [°]	2.1-25.0	2.1-25.0	0.9-25.0	2.4-25.0
Reflns collected	12999	13146	13855	13672
Reflns unique	8883	8942	4961	4888
Number of parameters	947	929	416	361
Independent reflections (R_{int})	0.048	0.036	0.112	0.174
R_1, wR_2 ($I > 2\sigma(I)$)*	0.0893, 0.2160	0.0919, 0.2383	0.0743, 0.1716	0.0906, 0.1987
R_1, wR_2 (all data)**	0.1424, 0.2490	0.1226, 0.2699	0.1127, 0.2061	0.1560, 0.2435

*$R = \sum(F_o - F_c)/\sum(F_o)$, **$wR_2 = \{\sum[w(F_o^2 - F_c^2)^2]/\sum(F_o^2)^2\}^{1/2}$.

Table 2. Selected bond distances (Å) and angles (deg) for **1-4**.

1			
Pr(1)-O(4)	2.426(15)	Pr(1)-O(5)	2.623(11)
Pr(1)-O(7)	2.798(14)	Pr(1)-O(8)	2.625(9)
Pr(1)-O(13)	2.612(11)	Pr(2)-O(1)	2.529(8)
Pr(2)-O(1W)	2.463(8)	Pr(2)-O(2)	2.523(8)
Pr(2)-O(10)	2.431(8)	Pr(2)-O(13)	2.453(11)
Pr(2)-O(14)	2.79(2)		
O(4)-Pr(1)-O(5)	52.6(4)	O(4)-Pr(1)-O(7)	113.7(6)
O(4)-Pr(1)-O(8)	109.1(4)	O(4)-Pr(1)-O(13)	75.1(5)
O(5)-Pr(1)-O(8)	63.4(2)	O(5)-Pr(1)-O(13)	117.3(3)
O(7)-Pr(1)-O(8)	47.1(4)	O(7)-Pr(1)-O(13)	71.9(4)
O(8)-Pr(1)-O(13)	115.9(3)	O(8)-Pr(1)-O(13)	115.9(3)
O(1)-Pr(2)-O(1W)	141.20(3)	O(1)-Pr(2)-O(2)	51.1(3)
O(1)-Pr(2)-O(10)	72.6(3)	O(1)-Pr(2)-O(13)	123.4(3)
O(1)-Pr(2)-O(14)	125.7(5)	O(1W)-Pr(2)-O(2)	136.1(3)
O(1W)-Pr(2)-O(10)	73.9(3)	O(1W)-Pr(2)-O(13)	88.3(3)
O(2)-Pr(2)-O(10)	76.7(3)	O(2)-Pr(2)-O(13)	75.0(3)
O(10)-Pr(2)-O(13)	114.4(3)		
2			
Nd(1)-O(1)	2.29(2)	Nd(1)-O(1W)	2.385(14)
Nd(1)-O(2)	2.609(11)	Nd(1)-O(4)	2.776(16)
Nd(1)-O(5)	2.614(12)	Nd(1)-O(7)	2.757(14)
Nd(1)-O(8)	2.628(9)	Nd(2)-O(14)	2.704(9)
Nd(2)-O(2)	2.440(11)	Nd(2)-O(2W)	2.447(9)
Nd(2)-O(5)	2.467(11)	Nd(2)-O(8)	2.481(9)
Nd(2)-O(10)	2.520(9)	Nd(2)-O(11)	2.518(8)
Nd(2)-O(13)	2.495(10)		
O(1)-Nd(1)-O(1W)	85.9(8)	O(1)-Nd(1)-O(2)	49.4(6)
O(1)-Nd(1)-O(4)	137.7(7)	O(1)-Nd(1)-O(5)	95.5(7)
O(1)-Nd(1)-O(7)	141.9(7)	O(1)-Nd(1)-O(8)	111.1(6)
O(1W)-Nd(1)-O(4)	130.1(6)	O(1W)-Nd(1)-O(5)	124.9(4)
O(1W)-Nd(1)-O(7)	57.2(6)	O(1W)-Nd(1)-O(8)	64.7(4)
O(5)-Nd(1)-O(7)	98.5(4)	O(5)-Nd(1)-O(8)	63.7(3)
O(2)-Nd(2)-O(2W)	88.8(4)	O(2)-Nd(2)-O(5)	67.4(4)
O(2)-Nd(2)-O(8)	68.4(3)	O(2)-Nd(2)-O(10)	74.5(3)
O(2)-Nd(2)-O(11)	122.4(3)	O(2)-Nd(2)-O(13)	134.7(4)
O(2W)-Nd(2)-O(5)	70.7(3)	O(2W)-Nd(2)-O(8)	137.9(3)
O(2W)-Nd(2)-O(10)	135.4(4)	O(2W)-Nd(2)-O(11)	141.3(3)
O(5)-Nd(2)-O(8)	68.0(3)	O(5)-Nd(2)-O(10)	133.3(3)
O(5)-Nd(2)-O(11)	139.0(4)	O(5)-Nd(2)-O(14)	103.3(3)
O(8)-Nd(2)-O(10)	73.6(3)	O(8)-Nd(2)-O(11)	79.2(3)
O(8)-Nd(2)-O(13)	77.0(4)	O(8)-Nd(2)-O(14)	123.2(3)
3			
Sm(1)-O(1)	2.464(8)	Sm(1)-O(1W)	2.370(9)
Sm(1)-O(2)	2.383(9)	Sm(1)-O(2W)	2.403(8)
Sm(1)-O(4)	2.527(8)	Sm(1)-O(5)	2.476(9)
Sm(1)-O(7)	2.418(9)	Sm(1)-O(8)	2.485(8)
O(1)-Sm(1)-O(2)	53.2(3)	O(4)-Sm(1)-O(8)	94.4(3)
O(1)-Sm(1)-O(1W)	75.1(3)	O(1)-Sm(1)-O(2W)	75.0(3)
O(1)-Sm(1)-O(4)	139.8(3)	O(1)-Sm(1)-O(5)	141.2(3)
O(1)-Sm(1)-O(7)	121.0(3)	O(1)-Sm(1)-O(8)	125.2(3)
O(1W)-Sm(1)-O(8)	79.0(3)	O(1W)-Sm(1)-O(2)	81.8(3)

O(1W)-Sm(1)-O(2W)	81.8(3)	O(1W)-Sm(1)-O(4)	125.0(3)
O(1W)-Sm(1)-O(5)	75.0(3)	O(1W)-Sm(1)-O(7)	130.5(3)
O(2)-Sm(1)-O(2W)	128.1(3)	O(2)-Sm(1)-O(4)	149.8(3)
O(2)-Sm(1)-O(5)	143.1(3)	O(2)-Sm(1)-O(7)	76.5(3)
O(2W)-Sm(1)-O(4)	74.6(3)	O(2W)-Sm(1)-O(5)	76.7(3)
O(2W)-Sm(1)-O(7)	145.1(3)	O(2W)-Sm(1)-O(8)	146.4(3)
4			
Tb(1)-O(1)	2.362(7)	Tb(1)-O(1W)	2.405(7)
Tb(1)-O(2)	2.443(7)	Tb(1)-O(2W)	2.326(7)
Tb(1)-O(4)	2.407(8)	Tb(1)-O(5)	2.473(7)
Tb(1)-O(7)	2.523(7)	Tb(1)-O(8)	2.465(7)
O(1)-Tb(1)-O(2)	53.1(2)	O(1)-Tb(1)-O(2W)	81.6(2)
O(1)-Tb(1)-O(4)	76.5(2)	O(1)-Tb(1)-O(5)	76.1(3)
O(1)-Tb(1)-O(7)	149.6(2)	O(1)-Tb(1)-O(8)	143.0(2)
O(1W)-Tb(1)-O(2W)	81.4(2)	O(1W)-Tb(1)-O(4)	145.6(2)
O(1W)-Tb(1)-O(5)	146.1(2)	O(1W)-Tb(1)-O(7)	75.0(2)
O(2)-Tb(1)-O(2W)	74.5(2)	O(2)-Tb(1)-O(4)	121.2(2)
O(2)-Tb(1)-O(5)	125.0(2)	O(2)-Tb(1)-O(7)	140.1(2)
O(2W)-Tb(1)-O(4)	130.5(2)	O(2W)-Tb(1)-O(5)	79.2(2)
O(2W)-Tb(1)-O(7)	125.6(2)	O(2W)-Tb(1)-O(8)	75.0(2)
O(4)-Tb(1)-O(7)	74.8(2)	O(4)-Tb(1)-O(8)	97.4(2)
O(3W)-H(3WD)···O(6)	0.9600	1.8300	2.795(17)	179.00
O(6) -H(6)··· O(3)	0.8200	1.9200	2.683(16)	155.00
4				
O(3)-H(3)···O(6)	0.8200	1.9700	2.746(12)	158.00
O(2W)-H(2WB)···O(2)	0.9600	1.8900	2.786(9)	154.00
O(6)-H(6)···O(3W)	0.8200	1.8100	2.601(12)	160.00
O(3W)-H(3WB)···O(9)	0.9600	2.1400	2.795(12)	124.00
O(1W)-H(1WA)···O(8)	0.9600	2.2900	2.798(9)	112.00

*$[H_3O][Nd_3(HPA)_{10}(H_2O)_3{\cdot}2H_2O]$ (**2**)*. Complex **2** was synthesized in a similar way as that for **1**, except that $Pr(NO_3)_3{\cdot}6H_2O$ was replaced by $Nd(NO_3)_3{\cdot}6H_2O$ (0.34 g, 0.75 mmol). Pink block crystals of **2** were obtained in 58% yield based on Nd. Anal. calc. for $C_{90}H_{102}O_{36}Nd_3$ (%): C, 49.30; N, 0; H, 4.69. Found: C, 49.43; N, 0; H, 4.63.

*$[Sm_2(HPA)_6(H_2O)_4{\cdot}2H_2O]$ (**3**)*. The solution of HHPA (0.125 g, 0.75 mmol) 20 mL CH_3OH:H_2O (v/v = 1:1) was added to an aqueous solution of $Sm(NO_3)_3{\cdot}6H_2O$ (0.34 g, 0.75 mmol), and then the mixture was heat to 60 ºC for 30 min. The pH of the resulting solution was adjusted to 6 using triethylamine and kept at room temperature. Yellow block crystals of **3** were obtained in 44% yield based on Pr. Anal. calc. for $C_{54}H_{66}O_{24}Sm_2$ (%): C, 46.33; N, 0; H, 4.75. Found: C, 46.49; N, 0; H, 4.70.

*$[Tb_2(HPA)_6(H_2O)_4{\cdot}2H_2O]$ (**4**)*. Complex **4** was synthesized in a similar way as that for **3,** except that $Eu(NO_3)_3{\cdot}6H_2O$ was replaced by $Tb(NO_3)_3{\cdot}6H_2O$ (0.34 g, 0.75 mmol). Colorless block crystals of **4** were obtained in 42% yield based on Tb. Anal. calc. for $C_{54}H_{66}O_{24}Tb_2$ (%): C, 45.77; N, 0; H, 4.70. Found: C, 45.88; N, 0; H, 4.65.

RESULTS AND DISCUSSION

Crystal structure description

*$[H_3O][Ln_3(HPA)_{10}(H_2O)_3{\cdot}2H_2O]$ (Ln = Pr for **1**, Ln = Nd for **2**)*. The determination of X-ray single crystal structures indicated that **1**-**2** are isostructural. Thus, the crystal structure of **1** will

be described only. In the asymmetric unit, each Pr(III) ion is coordinated to four μ_3-η^2:η^1 tridentate bridging carboxylate groups of HPA ligand and one water molecule. Two lattice water molecules are also present in the asymmetric unit. The coordination environment of the molecule shows that the Pr(II)/Nd ions are nine coordinated (Figure 1a-1b). The nine coordinated geometry arises when each Pr(II) ion is connected to the neighboring Pr(II) by the oxygen atoms of the carboxylate group in a bridging (μ_2) coordination mode. This type of arrangement generates Pr_2O_{16} chains (Figure 1c). The non-bonded distance between the two Pr(II) ions is 3.97 (2) Å. The packing of the molecule when viewed through the a-axis (Figure 1d) shows a porous structure in which some lattice water molecules are entrapped. This feature indicates that the pores generated in the molecule are hydrophilic in nature. The hydrogen atoms present in the lattice water, coordinated water, carboxylate group and the hydroxyl group of the HPA ligand are involved in hydrogen bonding thereby stabilizing the molecule. The hydrogen bonding pattern can be qualitatively viewed along c-axis (Figure 1e-1f). One of the hydrogen atoms of the hydroxyl group forms three hydrogen bonds with the carboxylic oxygen atoms, (O3–H3···O7, O1W–H1WC···O3, O9–H9···O3W), while the other hydrogen atoms form two hydrogen bonds with the carboxylic oxygen atoms of the water molecules (O1W–H1WA···O1,O2WA–H2WA···O5, O2WB–H2WB···O11) (Table 3). The three-dimensional framework of the molecules can be seen in the packing diagram viewed along *b*-axis (Figure 1d).

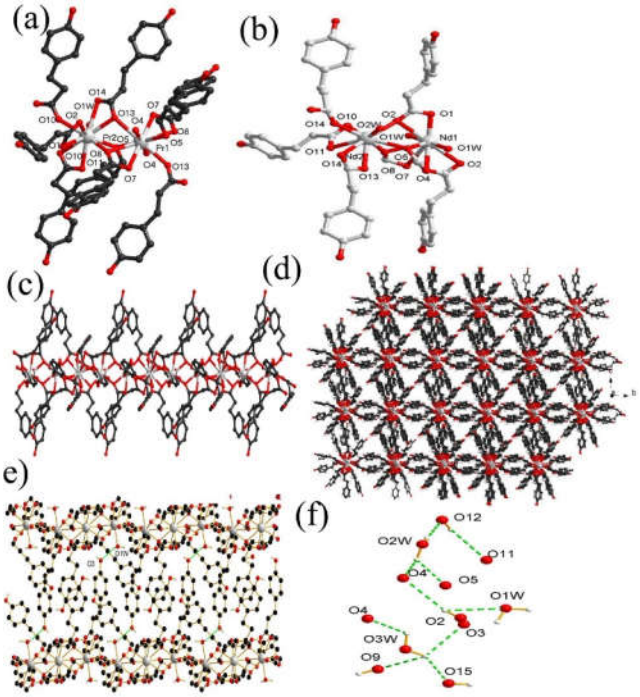

Figure 1. (a) The coordination geometry of Pr(III) ions in **1** (C: bronze, O: red, Pr: tint); (b) (a) the coordination geometry of Nd(III) ions in **2** (C: white, O: red, Pr: tint); (c) the 1D chain; (d) the packing 3D supramolecular network; (e) the H-bonded interactions between coordinated water molecules and hydroxyl group; (f) the different H-bonded types.

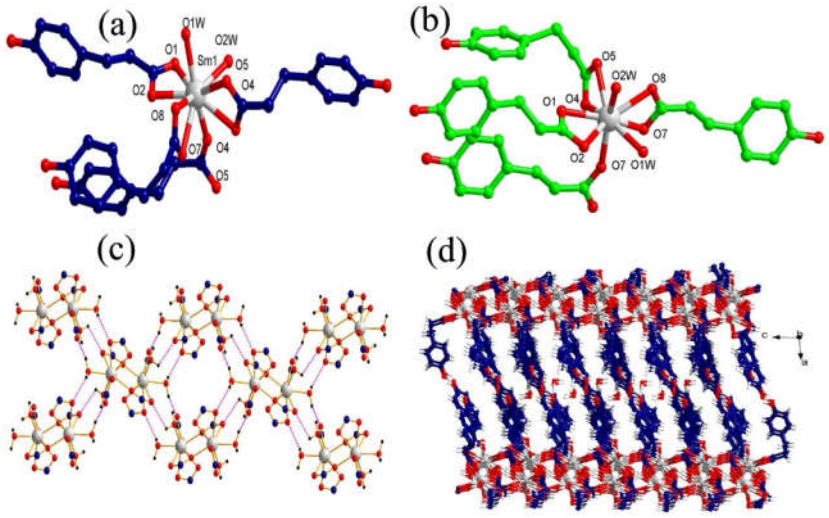

Figure 2. (a) The coordination geometry of Sm(III) ions in **3** (C: blue, O: red, Sm: tint); (b) the coordination geometry of Tb(III) ions in **4** (C: green, O: red, Tb: tint); (c) the H-bonded interactions among coordinated water molecules and hydroxyl groups; (d) the 3D supramolecular network in **3**.

*$[Ln_2(HPA)_6(H_2O)_4{\cdot}2H_2O]$ (Ln = Sm for **3**, Ln = Tb for **4**)*. X-Ray crystallographic study reveals that the structures of **3-4** are isostructural and are made up of neutral centrosymmetric dinuclear units which are further linked through hydrogen-bonding interactions to form a 3-D supramolecular network. The asymmetric unit of **3** consists of one Sm(III) center, three HPA ligands, two coordination water molecules and one free water molecule. The Sm(III) ion is nine-coordinated and exhibits distorted mono-capped square antiprism coordination geometry [12], which is surrounded by seven oxygen atoms from four distinct HPA ligands as well as two oxygen atoms from two coordination water molecules (Figure 2a-2b). For HPA ligands in **3-4**, all the carboxylate groups are deprotonated. There are two different types of coordination modes for HPA ligands: one links two Sm(III) ions by μ_1-η^1:η^1 bisdentate chelating carboxylate group; the other coordinates to one Sm(III) ion through the μ_3-η^2:η^1 tridentate bridging carboxylate group. In **3**, two adjacent Sm(III) ions are connected by four bridging HPA ligands to afford a centrosymmetric dinuclear unit with the Sm ··· Sm distance of 4.12 Å. Significantly, a careful analysis of this structure indicates that the O3–H3···O6 and O9–H9···O3 hydrogen bonds between hydroxyl group of HPA link the dinuclear units to generate a1-D chain. The O1W–H1WA···O8, O1W–H1WB···O4, O2W–H2WA···O5 and O2W–H2WB···O2 (Table 3) hydrogen bonds between the coordination water molecules and carboxylate oxygen of HPA ligands further connect the adjacent 1-D chains to generate the 3D layered net (Figure 2b-2c) [13]. The O9–H9C···O3W and O3W–H3WD···O6 hydrogen bonds between the free water molecule and hydroxyl group of HPA ligands further stabilize the full network.

Effects of temperature on the structure

Using a reaction of the same initial reactants and ratios, complexes **1-4** were synthesized at three temperatures of 80 and 60 °C, which show 1D and 0D structures, respectively. Evidently, with the temperature changed, complexes **1-4** exhibit different structures, although the coordination

modes of carboxylic acid ligand are same (Scheme 1). In addition, when the temperature is below 80 °C or in the range of 160−200 °C, no coordination polymer could be obtained. It is clear that the temperature plays an important role in the resulting products. Thus, CPs species that can be systematically tuned by one factor and undergo structural transformations still remain largely unexplored thus far, and this work presents a good case of temperature effects [2, 13].

Table 3. Selected the hydrogen bond distances (Å) for **1-4**.

Contact D–H···A	Distance, Å			Angle D–H···A, deg
	D–H	H···A	D···A	
1				
O(1W)-H(1WA)···O(1)	0.9600	1.7700	2.701(13)	162.00
O(1W)-H(1WC)···O(3)	0.9600	2.2800	2.825(14)	115.00
O(2)-H(3)··· O(7)	0.8200	2.2800	2.819(18)	124.00
O(2W)- H(2WA)···O(5)	0.9600	2.1200	2.750(3)	122.00
C(39)-H(39A)···O(7)	0.9300	2.3400	2.992(8)	127.00
O(3W)-H(3WB)···O(2)	0.9600	2.3700	2.804(17)	107.00
2				
O(2W)-H(2WA)···O(11)	0.9700	1.7900	2.729(13)	161.00
O(2W)-H(2WC)···O(12)	0.9600	2.4900	2.841(14)	102.00
O(3W)-H(3WA)···O(10)	0.9600	1.9900	2.772(19)	137.00
C(3) -H(3A)··· O(1)	0.9700	2.4100	2.790(4)	102.00
3				
O(1W)-H(1WB)···O(1)	0.9600	1.8800	2.777(11)	155.00
O(3)-H(3)···O(9)	0.8200	1.9400	2.712(17)	156.00
O(3W)-H(3WD)···O(6)	0.9600	1.8300	2.795(17)	179.00
O(6) -H(6)··· O(3)	0.8200	1.9200	2.683(16)	155.00
4				
O(3)-H(3)···O(6)	0.8200	1.9700	2.746(12)	158.00
O(2W)-H(2WB)···O(2)	0.9600	1.8900	2.786(9)	154.00
O(6)-H(6)···O(3W)	0.8200	1.8100	2.601(12)	160.00
O(3W)-H(3WB)···O(9)	0.9600	2.1400	2.795(12)	124.00
O(1W)-H(1WA)···O(8)	0.9600	2.2900	2.798(9)	112.00

TGA and PXRD

In order to study the thermal stabilities of **1-4**, the thermogravimetric analysis (TGA) were investigated under nitrogen atmosphere (Figure 3). For **1-2**, the first weight loss of 5.0% occurred between 35 and 135 °C, corresponding to the release of full H_2O molecules (calc. 4.9%). For **3-4**, the first weight loss of 7.3% occurred between 35 and 200 °C, corresponding to the release of full H_2O molecules (calc. 7.6%). With the temperature was above 215 °C, the frameworks of **1-4** started to decompose rapidly. In addition, the powder X-ray diffraction analyses of the frameworks of **1-4** were further conducted to confirm the phase purity of them. The PXRD patterns of the as-synthesized sample of **1-4** are in good agreement with their corresponding simulated patterns, which indicate the phase purity of the synthesized samples (Figure 4) [15].

Luminescence property

4 exhibits the resolved peaks of Tb^{3+} centered at 491, 545, 586, and 711 nm, respectively (Figure 5a), which result from the deactivation of the $5D_4$ excited state to the corresponding ^7F_J ground state of the Tb^{3+} cation (J = 6, 5, 4, 3). The most intense emission corresponds to the

hypersensitive transition of $^5D_4 \rightarrow {}^7F_5$ (545 nm). Among them, the symmetric forbidden emission band of $^5D_0 \rightarrow {}^7F_n$ around 581 nm is almost invisible [16-17].

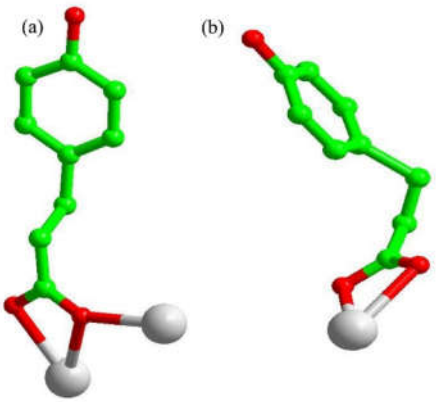

Scheme 1. The two types of coordination modes of HPA ligands in this work.

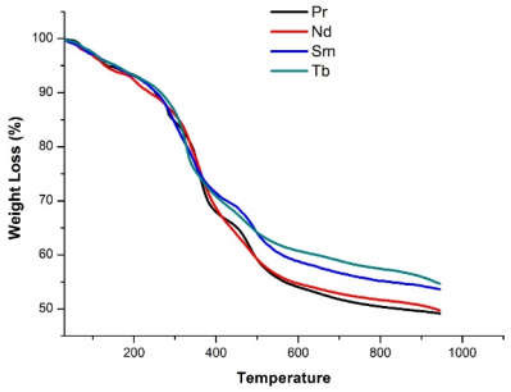

Figure 3. View of the TGA in **1-4**.

Sensing of metal ions and small organic molecules

The samples **4** was immersed in water solutions containing $M(NO_3)_x$ to form metal-ion-incorporated **1** as microcrystalline solids for luminescence studies. It is found that the d^{10}-based ions possessing a closed-shell electron configuration have a trivial effect on the luminescence intensity, whereas the other metal ions with different electron configurations produce varying degrees of quenching of the luminescence intensity, especially the Fe^{3+} ion (Figure 5b). It is very remarkable that this material features such highly selective and sensitive sensing of Fe^{3+} ion in water solution (Figure 5c). As for the reason of the quenching by Fe^{3+}, we speculate that it might be related to the interaction between the Fe^{3+} ions and the hydroxyl group Lewis basic sites on **4**, similar to that observed in the reported literature [18]. **2** is sensitive to the Fe^{3+} ion, the luminescent intensity of **4** decreased to 95% at 280 ppm (Figure 5c).

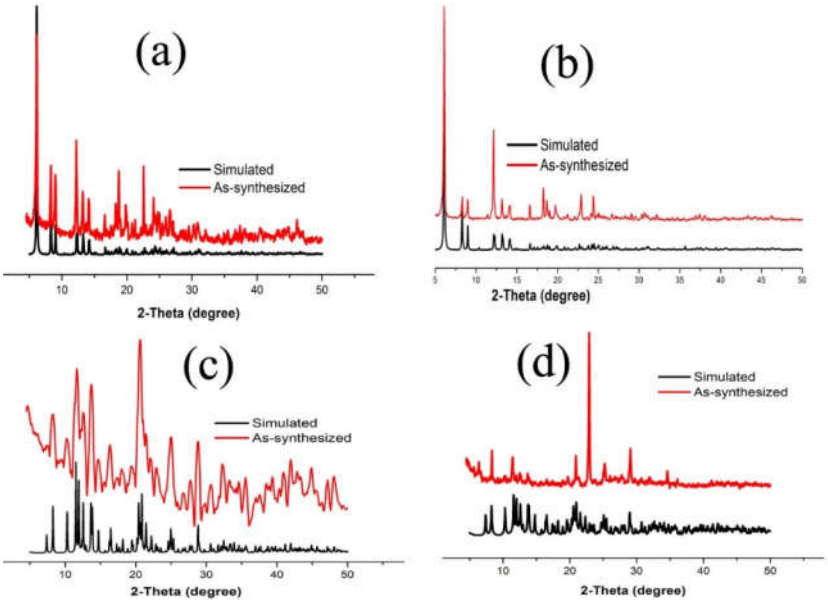

Figure 4. View of the PXRD patterns in **1-4**.

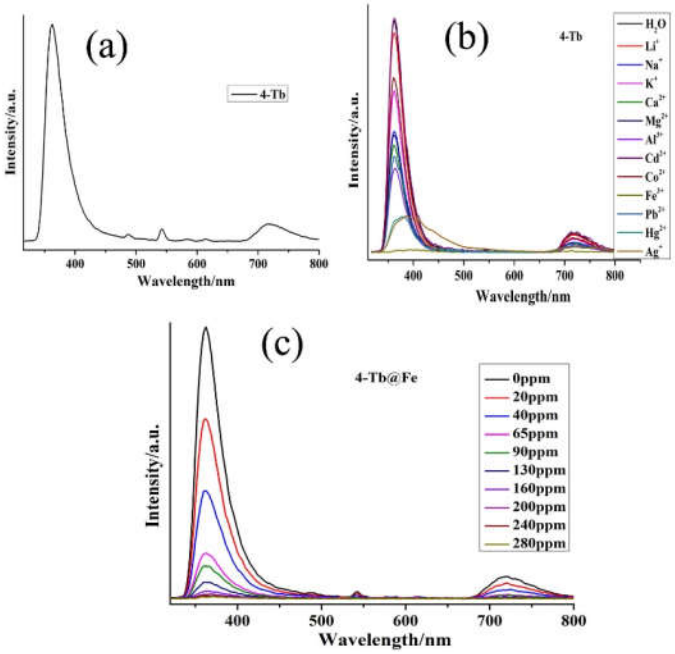

Figure 5. (a) the PL spectra of **4** under room temperature; (b) emission spectra of **4** after being immersed in various metal ions at 10^{-3} M at 298 K (excited at 305 nm); (c) emission spectra of **1** after being immersed in various concertation Fe^{3+} metal ions at 10^{-2} M (excited at 305 nm).

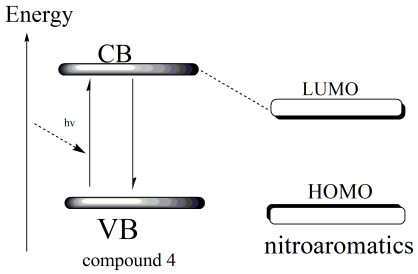

Scheme 1. Illustration of the electron transfer process between **4** and NACs.

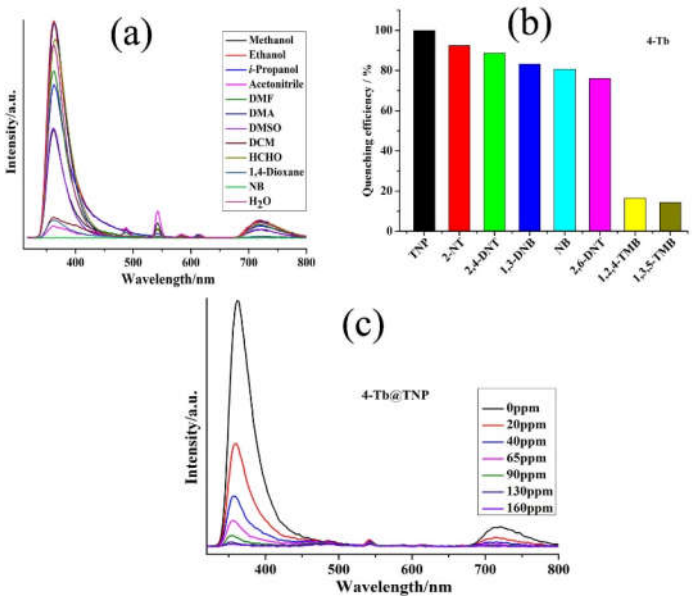

Figure 6. (a) Emission spectra of **1** after being immersed in various small organic molecule at 10^{-3} M at 298 K (excited at 305 nm); (b) luminescence quenching efficiency of **1** after adding different solvents; (c) emission spectra of **4** after being immersed in various concertation TNP at 298 K (excited at 305 nm).

To explore the potential applications of the polymers for probing organic small molecules, we tried to detect the effect of organic solvent on the luminescence properties of **1**. It was observed that the photoluminescence spectra of **1** are most dependent on the solvent molecules (Figure 6a), particularly in the case of nitrobenzene (NB), which exhibits the most significant quenching effects (Figure 6a). The possibility of a quenching mechanism of nitrobenzene may be caused by the electron-withdrawing properties of the nitro groups in the analyte [15]. The quenching effect of NB inspired us to further investigate other nitro-aromatics. The fluorescence properties of **4** suspensions in different nitro-aromatics were carried out. The results that show all the nitro-aromatic analytes can weaken the fluorescence intensity of **4** suspensions (Figure 6b). The most effective quencher is 2,4,6-trinitrophenol (TNP) with the maximum quenching

percentage. The luminescent intensity of **4** decreased to 98% at 160 ppm (Figure 6c). Following the 3δ/slope, the TNP detection limit is calculated to be 1.99 ppm [18-20]. The quenching constant and limit of detection for TNP by **4** were found to be comparable with the reported LMOF detection of TNP at the ppb level using MOFs [21-23], excluding the lowest detection limit so far reported, by Ghosh *et al.* (LOD = 2.9 ppb (12.9 nM, K_{SV} 4.6 × 104 M^{-1}) using bio-MOF) [23]. Therefore, **4** can be used to distinguish between nitroaromatics and aromatics with different electron-withdrawing/donor -NO_2 group groups. Considering the sizes of aromatic compounds and the structural feature, the possibility of the accommodation of these analytes in the pores of **4** can be ruled out. As mentioned earlier that the decline in luminescence intensity of MOFs in presence of NACs might be arising because of the charge transfer operating from photo-excited **4** towards the LUMO of analytes. This phenomenon operates when the LUMO of **4** is at higher energy level than that of the LUMOs of acceptor analytes. A simple schematic illustration of the electron transfer process was listed in Scheme 1 [24-25].

CONCLUSION

In summary, four new coordination polymers were successfully synthesized by using different temperature. The structural diversities of the complexes indicate that the temperature is an important factor for construction of coordination polymers with fascinating motifs. The luminescence properties of compound **4** implies that they may be good candidates for luminescent materials. It is anticipated that other related coordination polymers with various fascinating structures could be obtained in the future work.

ACKNOWLEDGMENTS

The authors acknowledge financial assistance from Sichuan University of Science and Engineering (nos. 2017RCL02), the Education Committee of Sichuan Province (nos. 18ZB0422 and 18ZB0425), the Department of Science and Technology of Sichuan Province (nos. 2017JY0129), the Project of Zigong Science & Technology (No. 2018YYJC01), the Opening Project of Key Laboratory of Green Chemistry of Sichuan Institutes of Higher Education (No: LZJ1705) and the Student's Platform for Innovation and Entrepreneurship Training Program (201810622053) and Special Funds for Scientific and Technological Innovation of undergraduates in Guangdong Province (pdjha2019b0221, pdjha2019b0222, pdjha2019b0219, pdjha2019b0215).

REFERENCES

1. Wang, Y.; Yang, J.; Liu, Y.Y.; Ma, J.F. Controllable syntheses of porous metal-organic frameworks: Encapsulation of Ln^{III} cations for tunable luminescence and small drug molecules for efficient delivery. *Chem. Eur. J.* **2013**, 19, 14591-14599.
2. Zhou, H.F.; He, T.; Yue, K.F.; Liu, Y.L.; Zhou, C.S.; Yan, N.; Wang, Y.Y. Temperature-induced syntheses, iodine elimination, enantiomers resolution, and single-crystal-to-single-crystal transformation of imidazole-Co(II) coordination polymers with amino-isophthalic acid as Co-ligand. *Cryst. Growth. Des*. **2016**, 16, 3961-3968.
3. Bu, X.H.; Chen, W.; Hou, W.F.; Du, M.; Zhang, R.H.; Brisse, F. Controlling the framework formation of silver(I) coordination polymers with 1,4-bis(phenylthio)butane by varying the solvents, metal-to-ligand ratio, and counteranions. *Inorg. Chem*. **2002**, 41, 3477-3482.
4. Dincă, M.; Yu, A.F.; Long, J.R. Microporous metal−organic frameworks incorporating 1,4-benzeneditetrazolate: Syntheses, structures, and hydrogen storage properties. *J. Am. Chem. Soc*. **2006**, 128, 8904-8913.

5. Liu, B.; Wei, L.; Li, N.N.; Wu, W.P.; Miao, H.; Wang, Y.Y.; Shi, Q.Z. Solvent/temperature and dipyridyl ligands induced diverse coordination polymers based on 3-(2′,5′-dicarboxylphenyl)pyridine. *Cryst. Growth. Des*. **2014**, 14, 1110-1127.
6. Cui, P.; Ren, L.J.; Chen, Z.; Hu, H.C.; Zhao, B.; Shi, W.; Cheng, P. Temperature-controlled chiral and achiral copper tetrazolate metal–organic frameworks: syntheses, structures, and I_2 adsorption. *Inorg. Chem*. **2012**, 51, 2303-2310.
7. Liu, X.M.; Xie, L.H.; Lin, J.B.; Lin, R.B.; Zhang, J.P.; Chen, X.M. Flexible porous coordination polymers constructed from 1,2-bis(4-pyridyl)hydrazine via solvothermal in *situ* reduction of 4,4′-azopyridine. *Dalton. Trans*. **2011**, 40, 8549-8554.
8. Zong, G.C.; Huo, J.X.; Ren, N.; Zhang, J.J., Qi, X.X.; Gao, J.; Geng, L.N.; Wang, S.P.; Shi, S.K. Preparation, characterization and properties of four new trivalent lanthanide complexes constructed using 2-bromine-5-methoxybenzoic acid and 1,10-phenanthroline. *Dalton. Trans*. **2015**, 44, 14877-14886.
9. Sessoli, R.; Powell, A.K. Strategies towards single molecule magnets based on lanthanide ions. *Coord. Chem. Rev*. **2009**, 253, 2328-2341.
10. Sheldrick, G.M. *SADABS, Program for Siemens Area Detector Absorption Corrections*, University of Göttingen: Germany; **1997**.
11. Roy, S.M.; Sudarsanakumar, M.R.; Suma, S.; Orathapachandra, K.; Dhanya, V.S.; Nair, R.M. Spectral, thermal and structural studies of an acetate bridged polymeric cadmium(II) complex: Poly[aqua(μ-acetato)(4-aminobenzoato)cadmium(II) monohydrate]. *Inorg. Chem. Comm*. **2014**, 40. 200-204.
12. Chen, M.; Hu, M.; Xu, W.M.; Saňudo, E.C.; Fang, S.M.; Liu, C.S. Six lanthanide supramolecular frameworks based on mixed *m*-/*p*-hydroxybenzoic acid and 1,10-phenanthroline tectons: Syntheses, crystal structures, and properties. *Polyhedron* **2016**, 113, 132-143.
13. Mishra, S.; Jeanneau, E.; Chermette, H.; Daniele, S.; Hubert-Pfalzgraf, L.G. Crystal-to-crystal transformations in heterometallic yttrium(III)–copper(I) iodide derivatives in a confined solvent-free environment: Influence of solvated yttrium cations on the nuclearity and dimensionality of iodocuprate clusters. *Dalton. Trans*. **2008**, 620-630.
14. Liu, J.Q.; Wu, J.; Wang, J.; Lu, L.; Daiguebonne, C.; Guillou, O.; Sakiyama, H.; Weng, N.S.; Zeller, M. Temperature identification on two 3D Mn(II) metal–organic frameworks: Syntheses, adsorption and magnetism. *RSC. Adv*. **2014**, 4, 20605-20611.
15. Wang, F.Q.; Wang, C.M.; Yu, Z.C.; Xu, K.H.; Li, X.Y.; Fu Y.Y. Two multifunctional Mn(II) metal-organic frameworks: Synthesis, structures and applications as photocatalysis and luminescent sensor. *Polyhedron* **2016**, 105, 49-55.
16. Zhu, Y.M.; Zeng, C.H.; Chu, T.S.; Wang, H.M.; Yang, Y.Y.; Tong, Y.X.; Su, C.Y.; Wong, W.T. A novel highly luminescent LnMOF film: a convenient sensor for Hg^{2+} detecting. *J. Mater. Chem. A* **2013**, 1, 11312-11319.
17. Guo, Z.Y.; Song, X.Z.; Lei, H.P.; Wang, H.L.; Su, S.Q.; Xu, H.; Qian, G.D.; Zhang, H.J.; Chen, B.L. A ketone functionalized luminescent terbium metal–organic framework for sensing of small molecules. *Chem. Commun*. **2015**, 51, 376-379.
18. Liu, J.Q.; Wu, J.; Li, F.M.; Liu, W.C.; Li, B.H.; Wang, J.; Li, Q.L.; Yadav, R.; Kumar, A. Luminescent sensing from a new Zn(II) metal–organic framework. *RSC. Adv*. **2016**, 6, 31161-31166.
19. Liu, J.Q.; Li, G.P.; Liu, W.C.; Li, Q.L.; Li, B.H.; Gable, R.W.; Hou, L.; Batten, S.R. Two unusual nanocage-based Ln-MOFs with triazole sites: Highly fluorescent sensing for Fe^{3+} and $Cr_2O_7^{2-}$, and selective CO_2 capture. *ChemPlusChem*. **2016**, 81, 1299-1304.
20. Li, B.H.; Wu, J.; Liu, J.Q.; Gu, C.Y.; Xu, J.W.; Luo, M.M.; Yadav, R.; Kumar, A.; Batten, S.R. A luminescent zinc(II) metal-organic framework for selective detection of nitroaromatics, Fe^{3+} and CrO_4^{2-}: A versatile threefold fluorescent sensor. *ChemPlusChem*. **2016**, 81, 885-892.

21. Song, X.Z.; Song, S.Y.; Zhao, S.N.; Hao, Z.M.; Zhu, M.; Meng, X.; Wu, L.L.; Zhang, H.J. Single-crystal-to-single-crystal transformation of a europium(III) metal-organic framework producing a multi-responsive luminescent sensor. *Adv. Funct. Mater.* 2014, 24, 4034-4041.
22. Nagarkar, S.S.; Desai, A.V.; Ghosh, S.K. A fluorescent metal–organic framework for highly selective detection of nitro explosives in the aqueous phase. *Chem. Commun*. **2014**, 50, 8915-8918.
23. Joarder, B.; Desai, A.V.; Samanta, P.; Mukherjee, S.; Ghosh, S.K. Selective and sensitive aqueous-phase detection of 2,4,6-trinitrophenol (TNP) by an amine-functionalized metal-organic framework. *Chem. Eur. J.* 2015, 21, 965-969.
24. Wang, F.M.; Wang, R.; Han, Y.Y.; Li, S.Y.; Man, J.H.; He, Y.X; Li, B.H. A microporous metal-organic framework with open metal sites for selective sensing Fe^{3+}, CrO_4^{2-} and nitrobenzene. *Bull. Chem. Soc. Ethiop*. **2017**, 31, 291-297.
25. Assefa, Z.; Gore, S.B. Stacking π-π Structural and spectroscopic studies of 2,9-dimethyl-1,10-phenanthrolinium cation (DPH) with chloride, triflate and gold dicyanide anions. The role of H-bonding in Molecular recognition and enhancement of p-p stacking. *Bull. Chem. Soc. Ethiop.* **2016**, 30, 231-239.